Metastability in Spin-Polarized Fermi Gases

Y. A. Liao, M. Revelle, T. Paprotta, A. S. C. Rittner, Wenhui Li, G. B. Partridge, and R. G. Hulet

Phys. Rev. Lett. **107**, 145305 — Published 28 September 2011

DOI: 10.1103/PhysRevLett.107.145305

Metastability in Spin-Polarized Fermi Gases

Y. A. Liao, M. Revelle, T. Paprotta,* A. S. C. Rittner,† Wenhui Li,‡ G. B. Partridge,§ and R. G. Hulet
Department of Physics and Astronomy and Rice Quantum Institute, Rice University, Houston, Texas 77005, USA

We study the role of particle transport and evaporation on the phase separation of an ultracold, spin-polarized atomic Fermi gas. We show that the previously observed deformation of the superfluid paired core is a result of evaporative depolarization of the superfluid due to a combination of enhanced evaporation at the center of the trap and the inhibition of spin transport at the normal-superfluid phase boundary. These factors contribute to a nonequilibrium jump in the chemical potentials at the phase boundary. Once formed, the deformed state is highly metastable, persisting for times of up to 2 s.

PACS numbers: 67.85.Lm, 67.10.Jn, 74.25.Ha, 03.75.Ss

The BCS theory of superconductivity is remarkably successful in describing pairing of unpolarized spin-1/2 particles. Pairing in spin-polarized systems is much more complicated, however, prompting speculation about exotic new pairing mechanisms that began shortly after the development of the BCS theory [1, 2], and continues until today [3, 4]. Spin-polarization, or more generally, imbalanced Fermi energies, arise in several physical situations including certain superconductors that support coexisting magnetic and superconducting order, color superconductivity in quark matter, and in ultracold atomic gases created with imbalanced spin populations. In 2006, a group at MIT [5, 6] and our group at Rice [7, 8] discovered that strongly-interacting spin-imbalanced trapped atomic gases undergo a first-order phase separation between a fully-paired superfluid core and lower density polarized regions.

There are significant qualitative and quantitative differences between the MIT and Rice experiments. The phase separation in the case of the Rice experiment was characterized by strong deformation of the paired core, in violation of the local-density approximation (LDA). In the LDA, the local chemical potentials $\mu_\sigma(\mathbf{r}) = \mu_\sigma - V(\mathbf{r})$ depend only on the trap potential $V(\mathbf{r})$ and the spatially-uniform global chemical potentials μ_σ. Here, $\sigma = \uparrow, \downarrow$ designate the two states of a pseudo-spin-1/2 system. The local densities are given by these local chemical potentials and the equilibrium equation of state of an infinite, spatially-uniform system. For a harmonically-confined gas with an unpolarized central core, the LDA implies a flat-topped axial spin-density (obtained by integrating the three-dimensional spin density along the two radial coordinates) [9–11]. While this flat-topped distribution was observed in the MIT experiment [6], in the Rice experiment the shape of the paired core was significantly less elongated than $V(\mathbf{r})$, resulting in a central dip in the axial spin-density [7, 8]. Furthermore, pairing in the Rice experiment was much more robust than in the MIT experiment, persisting to much larger population imbalances. This robust pairing is apparently in contradiction with the Clogston-Chandrasekhar limit describing the break-down of pairing when the difference between the chemical potentials of the two spin-states exceeds the pairing gap [12–15].

Possible explanations for this discrepancy have focused on the primary differences between the two experiments, which are trap aspect ratio and particle number [11, 16–21]. In both cases, the confining potential is approximately harmonic and elongated along the cylindrical (z) axis, as shown in Fig. 1(a). For the Rice experiment, however, the ratio of the radial to axial trap frequencies was ~30, while for MIT, it was ~5. Also, the total particle number in the Rice experiment was $\sim 10^5$, while for MIT, it was $\sim 5\times 10^6$. It was shown that while the observed deformation was consistent with the effect of a strong surface tension at the superfluid-normal interface [8, 16, 17], the required magnitude of the surface tension was inconsistent with detailed calculations [22, 23]. Furthermore, a recent experiment is largely in agreement with the MIT results despite having an aspect ratio and particle number that are similar to the Rice experiment [24]. A new mechanism has been proposed [25] which has its origins in the inhibition of thermal [26] and spin transport [25] across the phase boundaries coupled with an enhanced probability for evaporation at the axial center of the trap. These factors enable a distribution that is out of chemical equilibrium, where the difference in chemical potentials is depressed in the superfluid phase at trap center relative to the polarized normal phases in the wings. We have performed several experiments that strongly support this conjecture. In addition, we find that, once produced, the deformed state is remarkably metastable.

We produce imbalanced mixtures of ^{6}Li atoms as before in the two lowest energy hyperfine states ($F = 1/2$, $m_F = 1/2$) and ($F = 1/2$, $m_F = -1/2$), designated as states $|\uparrow\rangle$ and $|\downarrow\rangle$, respectively [7, 8]. A bias magnetic field is tuned to 834 G, corresponding to the unitary limit of the ^{6}Li Feshbach resonance. The atoms are confined in a hybrid optical-magnetic trap formed by a single focused laser beam propagating along the direction of the bias field (axial direction). Radial confinement is produced by the Gaussian intensity profile of the laser beam, while axial confinement arises from the combination of the Lorentzian axial profile of the laser beam and the residual magnetic curvature (confining) from the slightly non-Helmholtz configuration of the magnetic bias coils. This combination, depicted in Fig. 1(a), results in an aspect ratio of ~90 with an approximately isotropic trap depth when the

* Thorlabs Inc., Newton, NJ 07860
† The Boston Consulting Group, 20095 Hamburg, Germany
‡ Centre for Quantum Technologies, National University of Singapore, 3 Science Drive 2, Singapore, 117543
§ Agilent Technologies, Santa Clara, CA 95051

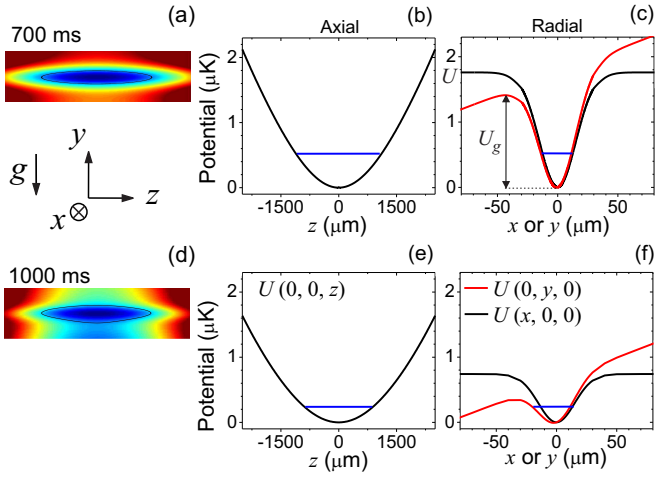

FIG. 1. (Color online) Plots of the hybrid magnetic-optical trap. Atoms are trapped at the focus of a laser beam propagating in the z (axial) direction. The laser wavelength is 1.08 μm and the beam is focused with a Gaussian beam waist ($1/e^2$ radius) of 30 μm. A residual magnetic curvature contributes to the axial confinement with a harmonic frequency of 3.8 Hz. (a)-(c) Optical trap depth $U = 1.68\,\mu$K, corresponding to $t = 700$ ms for the 1 s evaporation trajectory. U_g is the effective trap depth accounting for gravity. The relative contribution of the magnetic curvature and gravity are small. (d)-(f) Potential at the final optical trap depth $U_f = 0.74\,\mu$K at $t = 1$ s, where the relatively strong magnetic curvature has the effect of opening up a lip at $z = 0$. At this trap depth, the combined axial frequency, due to the optical and magnetic forces is 4.7 Hz. Values of $k_B T_F$ from Fig. 3(a) are indicated by the horizontal blue lines.

optical potential dominates. Evaporative cooling is effected by lowering the laser power, such that the trap depth, as well as the trap aspect ratio, are gradually reduced. At sufficiently low optical power the magnetic curvature dominates the axial confinement. When this happens, the trap depth becomes anisotropic, with the depth being largest along the axial (magnetic curvature) direction. Thus, a "lip" of minimum trap depth is formed in the radial direction at the axial trap center ($z = 0$), as shown in Fig. 1(d). Furthermore, gravity reduces the trap depth in the direction pointing downward in the lab (along $-y$).

Sequential absorption images [8] record the column density distributions of the trapped atoms for each state. Figure 2 shows representative axial density profiles, obtained by integrating the column density images along the remaining radial coordinate, for images recorded at various times along the evaporation trajectory used in our previous studies. For this trajectory, the trap depth was reduced exponentially as $e^{-t/\tau}$ from its initial value $U_i = 160\,\mu$K to a final value $U_f = 0.74\,\mu$K in a total time $t_{tot} = 1$ s, and with an exponential time constant $\tau = 200$ ms. Deformation is evidenced by a dip in the axial spin-density, which begins to develop at approximately $t = 700$ ms (Fig. 2(b)), corresponding to a temperature $T \simeq 0.2\,T_F$, where T_F is the Fermi temperature of a non-interacting trapped gas of $|\uparrow\rangle$ atoms. The deformation, characterized by the parameter $\alpha = n_v/n_p$ (see Fig. 3(c)), increases as the evaporation progresses and is maximum at t_{tot}, where $T \simeq 0.06\,T_F$ is at its minimum.

Figure 3 shows the progression of several relevant parameters during evaporation. U_g, shown in Fig. 3(a), is the trap depth including gravity, as defined in Fig. 1(c). Also shown in Fig. 3 are parameters extracted from a less aggressive evaporation trajectory for which $U_i = 160\,\mu$K as before, but now with $U_f = 2.2\,\mu$K, $t_{tot} = 3.4$ s, and $\tau = 500$ ms. This trajectory is designed to be similar to the final part of the trajectory used in Ref. [24], where no deformation was observed. Figure 3(b) shows the value of $\eta = (U_g - \epsilon_p)/k_B T$, where $\epsilon_p = {}^1/_2\, m\omega_z^2 R^2$, ω_z is the axial trap frequency, and R is the axial radius where the density of the majority state ($\uparrow$) goes to zero. The value of η is an approximate measure of the closeness of the chemical potential to the trap lip, and hence is related to the rate of evaporation. This quantity is significantly larger for the "gentle" 3.4 s trajectory as compared to the "aggressive" 1 s trajectory, indicating a much slower rate of evaporation. Nonetheless, even though the 3.4 s trajectory is not as deep or as aggressive, the final temperature of $\sim 0.09\,T_F$ is similar to that achieved with the 1 s trajectory. Furthermore, as shown in Fig. 4, the axial spin density at the end of the trajectory is flat-topped, indicating that there is no deformation even though the trap aspect ratio at the end of evaporation is highly elongated (aspect ratio of ~96). Deformation is prevented in the 3.4 s trajectory by its higher final trap depth, which both reduces the rate of evaporation and minimizes the lip at $z = 0$.

To determine whether the deformed state is only dynamically stable, existing only during rapid anisotropic evaporation, or rather, is a metastable state, we ramped the trap depth up over a time period of 600 ms following evaporation, as shown in Fig. 5(a). This serves to significantly suppress the rate of evaporation, as can be seen from the nearly constant value of T_F in Fig. 5(a) and the large values of η in Fig. 5(b). Nonetheless, Fig. 5(d), shows that the deformation α remains for more than 2 s following trap recompression. The degree of deformation is seen to decrease following recompression, roughly on the same timescale of an observed rise in the temperature.

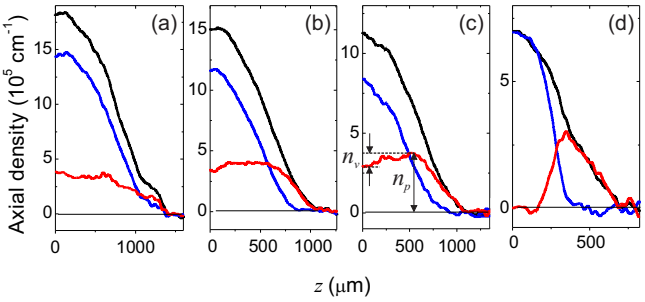

FIG. 2. (Color online) Axial densities taken at various times t along the evaporation trajectory. The global polarizations P are: (a) 600 ms, $P = 0.14$, (b) 700 ms, $P = 0.21$, (c) 740 ms, $P = 0.28$, (d) 1 s, $P = 0.18$. The variation in P is a result of shot-to-shot variations, as each image requires the trap to be reloaded and evaporated to the specified t. The upper (black) curves correspond to the majority state ($|\uparrow\rangle$), the middle (blue) curves to the minority state ($|\downarrow\rangle$), and the axial spin-densities are ($|\uparrow\rangle - |\downarrow\rangle$) are given by the lower (red) curves.

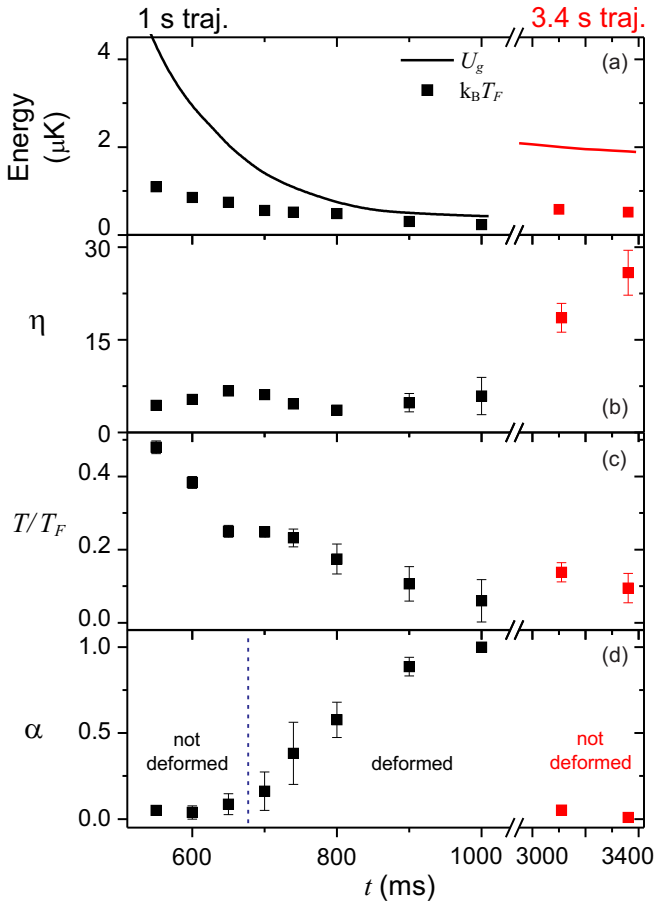

FIG. 3. (Color online) Parameters extracted from the axial densities for both the (aggressive) 1 s and (gentle) 3.4 s trajectories. T is determined from unpolarized ($P = 0$) distributions which are separately evaporated using the same trajectory. The mean energy E of these distributions is obtained from their mean-squared radius via the virial theorem [27]. The E vs. T calibration is given in Ref. [28] and is based on the experimental data of Ref. [29]. $\eta = (U_g - \epsilon_p)/k_B T$, where $\epsilon_p = {}^1/_2\, m\omega_z^2 R^2$, ω_z is the axial trap frequency, and R is the axial radius where the density of the majority state (↑) goes to zero. The deformation parameter is defined as $\alpha = n_v/n_p$, as depicted in Fig. 2(c). The error bars are mainly statistical uncertainty from the average of ~6 shots of various value of P at each value of t. The vertical dashed line in (d) indicates the onset of deformation.

Another measure of the effect of the lip in the potential may be obtained by axially displacing the center of the magnetic curvature with respect to the focus of the optical trap laser beam, as depicted in Fig. 6. Since the lip is located at the minimum of the magnetic curvature ($z = z_m$), its position no longer coincides with the overall minimum of the combined magnetic/optical potential, indicated by z_0 in Fig. 6. Figure 6 shows that while the unpaired atoms, given by the distribution of $|{\uparrow}\rangle - |{\downarrow}\rangle$, reside near the center of the combined potential (z_0), the paired core, given by the $|{\downarrow}\rangle$ distribution, displaces towards the lip at $z = z_m$ where evaporative cooling has maximum effect. This observation provides a graphic illustration of the lack of equilibration between the superfluid core and the normal phases.

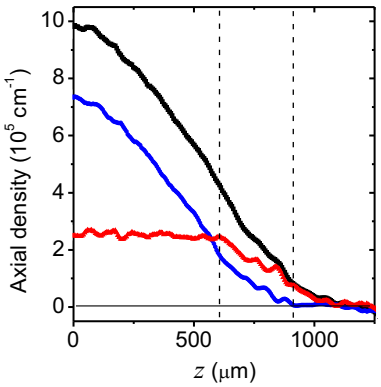

FIG. 4. (Color online) Axial densities for the 3.4 s trajectory at t = 3.4 s, with $P = 0.24$. Curve designations are the same as in Fig. 2. The dashed vertical lines indicate the location of phase boundaries. The flat-topped axial spin-density is consistent with the LDA, even though the aspect ratio of the trap potential is ~96.

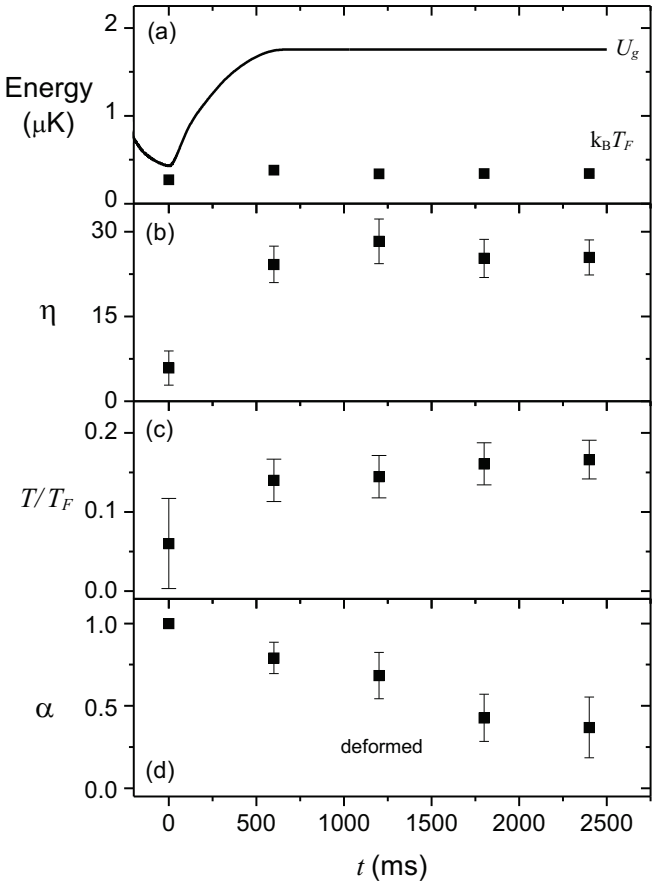

FIG. 5. Recompression of the trap following the 1 s evaporation. Here, the 1 s evaporation finishes at $t = 0$ and is followed by a slow recompression of the trap over the next 0.6 s. Even though the final value of U_g is similar to that shown for the 3.4 s trajectory in Fig. 3 the recompressed values of T_F are lower due to smaller overall numbers (~3×10^4 vs. ~10^5).

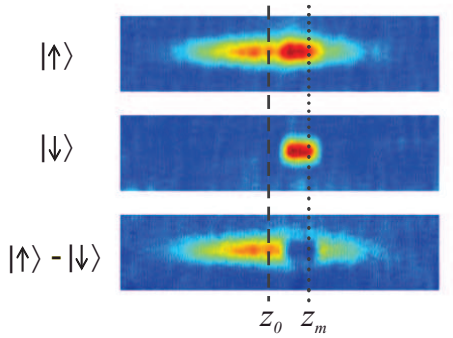

FIG. 6. (Color online) Column density images for an axial displacement of the center of magnetic curvature located at $z_m = 0$ and indicated by the dotted vertical line, from the focus of the optical trap beam located at $z = -1$ mm. At this trap depth ($U = 0.65\,\mu$K), the center of the combined potential, indicated by the dashed vertical line, is located at $z_0 = -210\,\mu$m. The trap beam waist is $26\,\mu$m and the residual magnetic curvature is 6.4 Hz for this data. The image size is $1653\,\mu\text{m} \times 100\,\mu$m and $P = 0.63$. The uncertainty in z_0 and z_m is $20\,\mu$m due to uncertainties in the optical trap parameters.

We have presented a series of measurements that are consistent with a model of evaporative depolarization [25]. In this model, the chemical potential of the majority species is depleted by preferential evaporation in the vicinity of a lip in the elongated trap potential. Because of the inhibition of spin transport, for sufficiently fast evaporation the chemical potential difference can be smaller in the paired core than in the polarized wings. This helps to stabilize the superfluid phase beyond the Clogston-Chandrasekhar limit, as was observed experimentally [7, 8]. The absence of a spatial variation in the spin-density of the superfluid phase [8] shows that the gradient in the chemical potential difference is not smoothly varying, but rather that it undergoes a sudden jump at the phase boundary. This indicates that the interface, not the bulk superfluid, is the dominate obstacle to spin transport. Slow relaxation of a non-equilibrium spin distribution in a spin-imbalanced phase separated gas was also reported in Ref. [30]. The observed relaxation time scales in that experiment are consistent with ours but the relative importance of the interface compared with the bulk superfluid could not be determined. (A previous experiment also reported slow diffusion but it was conducted with a balanced spin mixture, and hence without phase boundaries [31]). In our experiment, the jump in the local chemical potential difference at the phase boundary strongly deforms the shape of the superfluid-normal interface, making it much less curved than it would be at equilibrium. This nonequilibrium distribution is remarkably metastable, consistent with the calculations presented in Ref. [21], in which they find both LDA-like solutions as well as nearly degenerate LDA-violating ones whose density distributions closely resemble those that we observe.

We thank David Huse and Henk Stoof for valuable discussions. This work was supported under ARO Award W911NF-07-1-0464 with funds from the DARPA OLE program, and by the NSF, the ONR, and the Welch Foundation (grant C-1133).

[1] P. Fulde and R. A. Ferrell, Phys. Rev. **135**, A550 (1964).
[2] A. I. Larkin and Y. N. Ovchinnikov, Sov. Phys. JETP **20**, 762 (1965).
[3] R. Casalbuoni and G. Nardulli, Rev. Mod. Phys. **76**, 263 (2004).
[4] D. E. Sheehy and L. Radzihovsky, Annals of Physics **322**, 1790 (2007).
[5] M. W. Zwierlein, A. Schirotzek, C. H. Schunck, and W. Ketterle, Science **311**, 492 (2006).
[6] Y. Shin, M. W. Zwierlein, C. H. Schunck, A. Schirotzek, and W. Ketterle, Phys. Rev. Lett. **97**, 030401 (2006).
[7] G. B. Partridge, W. Li, R. I. Kamar, Y. A. Liao, and R. G. Hulet, Science **311**, 503 (2006).
[8] G. B. Partridge, W. Li, Y. A. Liao, R. G. Hulet, M. Haque, and H. T. C. Stoof, Phys. Rev. Lett. **97**, 190407 (2006).
[9] T. N. De Silva and E. J. Mueller, Phys. Rev. A **73**, 051602 (2006).
[10] M. Haque and H. T. C. Stoof, Phys. Rev. A **74**, 011602 (2006).
[11] A. Imambekov, C. J. Bolech, M. Lukin, and E. Demler, Phys. Rev. A **74**, 053626 (2006).
[12] B. S. Chandrasekhar, Appl. Phys. Lett. **1**, 7 (1962).
[13] A. M. Clogston, Phys. Rev. Lett. **9**, 266 (1962).
[14] C. Lobo, A. Recati, S. Giorgini, and S. Stringari, Phys. Rev. Lett. **97**, 200403 (2006).
[15] Y. Shin, C. H. Schunck, A. Schirotzek, and W. Ketterle, Nature **451**, 689 (2008) .
[16] T. N. De Silva and E. J. Mueller, Phys. Rev. Lett. **97**, 070402 (2006).
[17] M. Haque and H. T. C. Stoof, Phys. Rev. Lett. **98**, 260406 (2007).
[18] R. Sensarma, W. Schneider, R. B. Diener, and M. Randeria, arXiv:0706.1741 (2007).
[19] M. Tezuka, Y. Yanase, and M. Ueda, arXiv:0811.1650v3 (2010).
[20] M. Ku, J. Braun, and A. Schwenk, Phys. Rev. Lett. **102**, 255301 (2009).
[21] L. O. Baksmaty, H. Lu, C. J. Bolech, and H. Pu, Phys. Rev. A **83**, 023604 (2011).
[22] S. K. Baur, S. Basu, T. N. De Silva, and E. J. Mueller, Phys. Rev. A **79**, 063628 (2009).
[23] J. Diederix, K. Gubbels, and H. T. C. Stoof, in *The BCS-BEC Crossover and the Unitary Fermi Gas (Lecture Notes in Physics)*, edited by W. Zwerger (Springer, 2011).
[24] S. Nascimbène, N. Navon, K. J. Jiang, L. Tarruell, M. Teichmann, J. McKeever, F. Chevy, and C. Salomon, Phys. Rev. Lett. **103**, 170402 (2009).
[25] M. M. Parish and D. A. Huse, Phys. Rev. A **80**, 063605 (2009).
[26] B. Van Schaeybroeck and A. Lazarides, Phys. Rev. Lett. **98**, 170402 (2007); Phys. Rev. A **79**, 053612 (2009).
[27] L. Luo and J. E. Thomas, J. Low Temp. Phys. **154**, 1 (2009).
[28] H. Hu, X.-J. Liu, and P. D. Drummond, New J. Phys. **12**, 063038 (2010).
[29] S. Nascimbène, N. Navon, K. J. Jiang, F. Chevy, and C. Salomon, Nature **463**, 1057 (2010).
[30] A. Sommer, M. Ku, and M. W. Zwierlein, New J. Phys. **13**, 055009 (2011).
[31] A. Sommer, M. Ku, G. Roati, and M. W. Zwierlein, Nature **472**,

201 (2011).